

# Laser plasma accelerated ultra-intense electron beam for efficiently exciting nuclear isomers

Jie Feng,<sup>1,2</sup> YaoJun Li,<sup>1,2</sup> JunHao Tan,<sup>1,2</sup> WenZhao Wang,<sup>1,2</sup> YiFei Li,<sup>3</sup> XiaoPeng Zhang,<sup>4</sup> Yue Meng,<sup>1</sup> XuLei Ge,<sup>1,2</sup> Feng Liu,<sup>1,2</sup> WenChao Yan,<sup>1,2</sup> ChangBo Fu,<sup>5</sup> LiMing Chen,<sup>1,2,\*</sup> and Jie Zhang<sup>1,2,3,†</sup>

<sup>1</sup>*Key Laboratory of Laser Plasma (MoE), School of Physics and Astronomy, Shanghai Jiao Tong University, Shanghai 200240, China*

<sup>2</sup>*IFSA Collaborative Innovation Center, Shanghai Jiao Tong University, Shanghai 200240, China*

<sup>3</sup>*Laboratory of Optical Physics, Institute of Physics, Chinese Academy of Sciences, Beijing 100190, China*

<sup>4</sup>*Institute of High Energy Physics, Chinese Academy of Sciences, Beijing 100049, China*

<sup>5</sup>*Key Laboratory of Nuclear Physics and Ion-beam Application (MoE), Institute of Modern Physics, Fudan University, Shanghai 200433, China*

(Dated: March 15, 2022)

Utilizing laser plasma wakefield to accelerate ultra-high charge electron beam is critical for many pioneering applications, for example to efficiently produce nuclear isomers with short lifetimes which may be widely used. However, because of the beam loading effect, electron charge in a single plasma bubble is limited in level of hundreds picocoulomb. Here, we experimentally present that a hundred kilo-ampere, twenty nanocoulomb, tens of MeV collimated electron beam is produced from a chain of wakefield acceleration, via a tightly focused intense laser pulse transversely matched in dense plasma. This ultra-intense electron beam ascribes to a novel efficient injection that the nitrogen atom inner shell electrons are ionized and continuously injected into multiple plasma bubbles. This intense electron beam has been utilized to exciting nuclear isomers with an ultra-high peak efficiency of  $1.76 \times 10^{15}$  particles/s via photonuclear reactions. This efficient production method of isomers can be widely used for pumping isotopes with excited state lifetimes down to picosecond, which is benefit for deep understanding nuclear transition mechanisms and stimulating gamma-ray lasers.

## I. INTRODUCTION

The laser plasma wakefield accelerators (LWFAs) have attracted significant interests in recent years[1–4] due to high acceleration gradients (hundreds of GV/m) and beam current (tens of kilo-ampere), thus not only enable GeV electron accelerators reducing to a length of centimeters[5], but drive secondary radiation/particle sources with ultra-high brightness/flux[6–8]. In bubble[9] or blowout[10] regime LWFAs, an ultra-short intense laser pulse excites wakefield in underdense plasma, and the laser ponderomotive force expels electrons forming ion cavities (or called bubbles) in which electrons can be accelerated. In the last decade, some breakthroughs of LWFAs have been achieved such as ultra-high stability[11], multi-GeV energy[12], femtosecond (fs) beam duration[13], ultra-low energy spread[7, 14] etc., but beam charge is limited below hundred picocoulomb (pC).

Recently, several hundred pC electron beams have been observed in the process of double self-injection[15, 16] and self-truncated ionization injection[17–20] respectively, but it is still difficult to reach nanocoulomb (nC) due to the beam loading effect of bubble regime[10, 21, 22]. There are also some efforts in improving beam charge by increasing laser energy and using high-Z gas[23–26], but they still do not break through the limitation of beam loading effect. While self-modulated laser wakefield acceleration (SM-LWFA)[27–30] that long laser pulse overlaps with several tens of plasma waves, large number of

electrons can be trapped and accelerated in every wakefield and the beam charge can be increased tremendously to tens of nC[31, 32], but it requires a hundred joule class picosecond (ps) laser facility. Moreover, directional electron beams with tens of nC charge have also been produced via vacuum laser acceleration with a plasma mirror injector[33, 34]. Unfortunately, the beam collimation suffers from the ponderomotive force of the laser pulse in vacuum during acceleration, which results in a large divergence angle ( $\sim 20^\circ$ ) and a hole in the beam profile[35]. By way of contrast, a hundred nC collimated ( $\sim 3^\circ$ ) electron beam has been acquired from laser solid interactions with deliberately induced pre-plasma[36]. Although laser solid interaction is propitious to realize ultra-high charge, an important limited factor is the acceleration distance resulting in electron energy usually less than 10 MeV. Moreover, tens of nC electron beam with higher energy gain can also be realized in LWFA of near-critical-density plasma[37–39], but the beam divergence angle is usually large ( $\sim 15^\circ$ ) due to electrons interaction with laser fields, and they would also scatter in dense plasma after the laser pulse rapid depletion. In general, for laser plasma electron acceleration, it is a great challenge to realize electron beam with large charge, tight collimation and high energy at the same time.

In this work, the electron beams with charge of  $\sim 20$  nC and small divergence angle  $\sim 6^\circ$  have been generated experimentally from a tens of TW tightly focused laser pulse interacting with high density gas. Particle in cell simulation shows that a novel and efficient electron injection scenario of electrons successively ionization

injecting into multiple bubbles has been realized, resulting in super-high charge surpassing the scaling law[40] of LWFA in bubble regime. The electron beams generated have appropriate energies (10s MeV) for driving photonuclear reactions and nuclear isomers production. So, these dense and energetic electron beams hit on Indium target, and a significant amount of multiple isomers have been produced with an ultra-short time duration. This opens a new path to produce nuclear isomers with an extremely high peak efficiency.

## II. EXPERIMENTAL SETUP

The experiment is carried out using a Ti: Sapphire laser system at the Laboratory of Laser Plasmas of Shanghai Jiao Tong University. The experimental setup is shown in Fig. 1. A linearly polarized laser pulse with duration of 45 fs (FWHM), energy of 3.2 J is focused by an f-number 4 off-axis parabolic (OAP) mirror onto a supersonic gas jet[41], with well-defined uniform density distribution. The laser pulse can be focused to a main spot with radius  $w_0 = 3.8\mu\text{m}$ , containing about 38% of

the laser power, i.e.,  $\sim 27\text{ TW}$ , resulting in an intensity of  $\sim 5.8 \times 10^{19}\text{ W/cm}^2$ , corresponding normalized vector potential  $a_0 \approx 4.9$ . By regulating the gas back pressure, the outflow nitrogen gas density can range from  $3 \times 10^{17}\text{ cm}^{-3}$  to  $2 \times 10^{19}\text{ cm}^{-3}$ . After the laser interaction with pure nitrogen gas, the accelerated electron beam bombards a 1 mm-thick tungsten (W) converter which is located at the downstream of nozzle to generate bremsstrahlung radiation. Then the collimated  $\gamma$ -ray induces the  $(\gamma, \gamma')$  reaction, photofission  $(\gamma, n)$ ,  $(\gamma, 2n)$ ,  $(\gamma, 3n)$  reactions, and the followed neutron capture  $(n, \gamma)$  reaction in a 3 mm-thick indium (In) converter. These products of above reactions would be in nuclear isomeric states or become radionuclides, which can be identified by measuring their characteristic decay radiations with a high pure germanium detector.

## III. EXPERIMENTAL RESULTS

*Efficient electron acceleration.* Laser pulse focused by a small  $f$ -4 OAP has intense power density but shorter Rayleigh length  $l_R \approx 60\mu\text{m}$  for  $w_0 = 3.8\mu\text{m}$ . Due to the plasma bubble radius and the laser self-focusing power  $P_c \approx 17n_c/n_e[\text{GW}]$ , where  $\omega_{pe} = \sqrt{4\pi n_e e^2/m_e}$  is plasma frequency and  $n_c$  is critical density, a higher density plasma is usually required to match the small laser focal spot ( $w_0 \approx R$ ) for maintaining laser intensity and overcoming quick defocus[40]. Because 27 TW focused laser pulse is hard to self-focusing in the plasma at density of about  $5.6 \times 10^{18}\text{ cm}^{-3}$  corresponding  $P_c = 52\text{ TW}$ , so an electron beam with multiple spots and low energy is generated, as results shown in Figs. 2(a), 2(e); When plasma density is increased to  $1.12 \times 10^{19}\text{ cm}^{-3}$  ( $P_c = 26\text{ TW}$ ), the matched laser  $w_0 \approx R \approx 6\mu\text{m}$  during self-focusing and  $a_0 \approx 3$  is higher than the intensity of ionization threshold of nitrogen inner shell electrons[42, 43]. The electron beam charge is increased prominently to about 5 nC, far exceeding the charge scaling law of nonlinear bubble regime[44] (the detail mechanism to be discussed later); With the increase of plasma density to  $3.68 \times 10^{19}\text{ cm}^{-3}$  ( $P_c = 8\text{ TW}$ ), electron beam charge could be up to 20 nC and the divergence angle is just  $\sim 6^\circ$  [Figs. 2(c), 2(f)]. However, further increase plasma density, all of electron beam parameters deteriorate [Figs. 2(d-f)], due to the aggravated dephasing of electrons and the faster depletion of laser pulse in higher density plasma. It is worthy to mention that the optimal energy conversion efficiency from laser to collimated electron beam could be up to 12.4% for  $E_k > 1\text{ MeV}$  [Fig. 2(g)], when the small focal spot laser pulse is matched by a suitable density plasma. Moreover, the beam energy is mainly located in the range of 5~30 MeV, which is ideal to drive  $\gamma$ -rays for stimulating photonuclear reactions in the giant dipole resonance region[45].

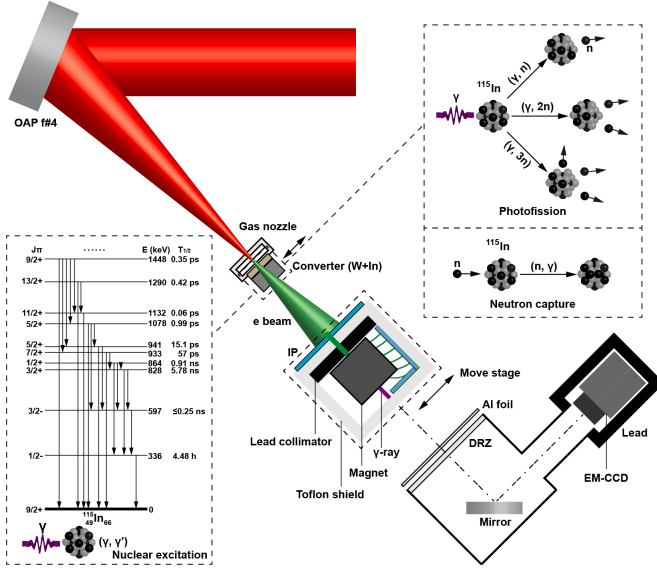


FIG. 1. Experimental setup. The femtosecond laser pulse is focused onto the front edge of supersonic gas nozzle which has 10 mm length, 1.2 mm opening width. Electron beam bombards DRZ fluorescent screen (covered with  $14\mu\text{m}$  Al film to block stray light) emitting fluorescence, which is detected by an EM-CCD to get electron beam spot image. When move in magnet, the electron beam energy spectrum is recorded by SR-type image plates (IPs). When move in converter (W+In), electron beam drives photofission reactions  $(\gamma, xn)$  and photonuclear excitation  $(\gamma, \gamma')$ . The generated neutrons can also induce neutron capture reaction  $(n, \gamma)$  in converters. Due to the converter (In) has two natural isotopes  $^{115}\text{In}$  (95.71%) and  $^{113}\text{In}$  (4.29%), here only shows the schematics of photofission, neutron capture and the excited states of  $^{115}\text{In}$  nucleus.

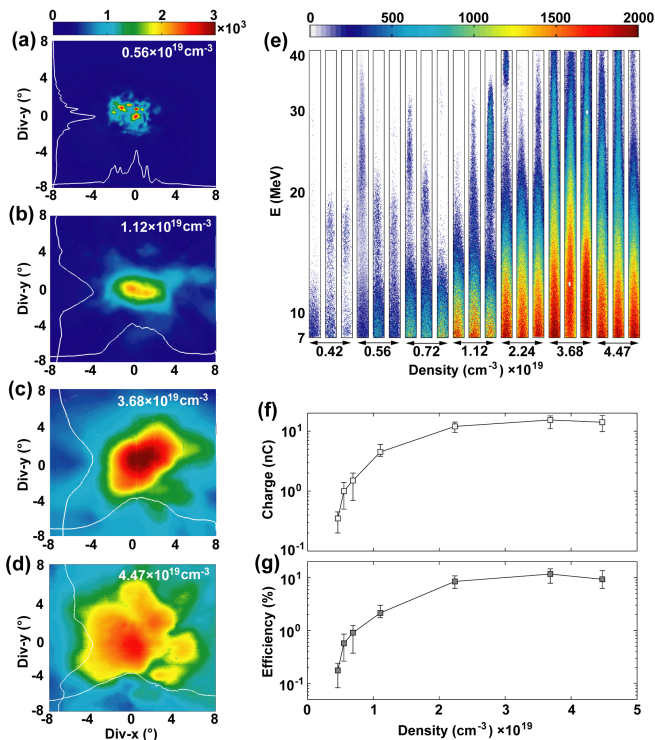


FIG. 2. Experimental results of electron beam for different density plasma. (a-d) Electron beam angular distributions at plasma densities of  $0.56$ ,  $1.12$ ,  $3.68$  and  $4.47 \times 10^{19} \text{cm}^{-3}$  respectively. (e) Electron beam energy distributions at different plasma densities. (f) and (g) is the corresponding total charge ( $E > 1 \text{ MeV}$ ) and energy conversion efficiency of laser to electron beam respectively.

*Electron beam stabilities.* To better demonstrate the characteristics of this optimized high efficiency laser plasma accelerator, electron beam stabilities, including energy spectrum, pointing, divergence angle and charge, are summarized as follow. The electron beam energy spectrums of continuous 10 shots are shown in Fig. 3(a). It is fitted by using double temperature  $T_{e1} = 1.19 \pm 0.19 \text{ MeV}$ ,  $T_{e2} = 12.88 \pm 2.41 \text{ MeV}$ , and the ratio of the total number of electrons in the two temperatures is  $N_1/N_2 = 23.90 \pm 5.42$ , here the error bars represent the standard deviation. The electron beam pointing stability of continuous 70 shots detected by DRZ is shown in Fig. 3(b), the standard deviation at x and y direction is  $4.14 \text{ mrad}$  and  $5.09 \text{ mrad}$  respectively. The corresponding divergence angle at x and y direction is  $7.0^\circ \pm 1.2^\circ$  and  $6.1^\circ \pm 1.3^\circ$  respectively [Fig. 3(c)]. Moreover, the electron beam charges are shown in Fig. 3(d), the average charge is  $15.59 \pm 1.68 \text{ nC}$ .

#### IV. SIMULATION AND ANALYSIS

*Particle in Cell Simulation.* The two-dimensional particle in cell simulations were carried out using the

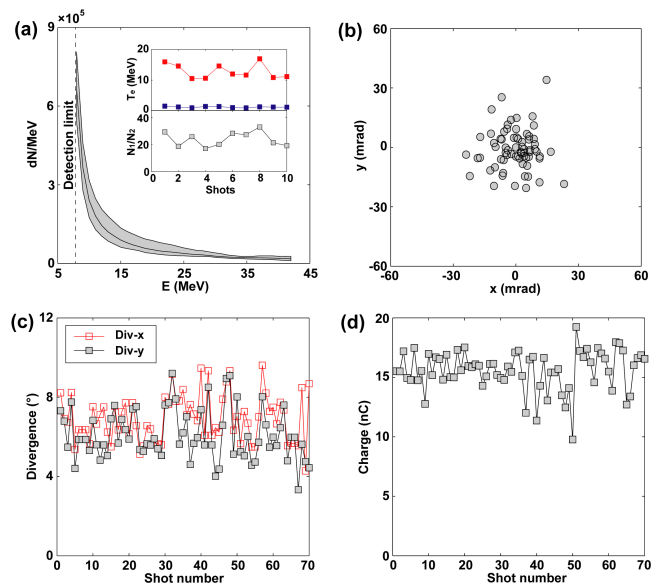


FIG. 3. Experimental electron beam stabilities. (a) Electron beam energy spectrum of continuous 10 shots. The inset shows the temperatures of double temperature fitting and the ratio of the total number of electrons in the two temperatures. (b) Electron beam pointing of continuous 70 shots. (c) Electron beam divergence angle. (d) Electron beam charge.

EPOCH code[46]. The simulation box size is  $120 \times 120 \mu\text{m}^2$  with  $4800 \times 1200$  cells in the x and y directions. The simulation box propagates along the x-axis at the speed of light. Ionization is modelled with the ADK rates, one macro-particle per cell is used as nitrogen atom. The neutral nitrogen longitudinal profile has a  $100 \mu\text{m}$  up-ramp followed by a  $1.2 \text{ mm}$  long plateau with a uniform density, then followed by a  $100 \mu\text{m}$  down-ramp. The p-polarized laser pulse propagates along the x-direction, and the laser-focusing plane is located at the middle of up-ramp. The laser pulse has a Gaussian transversal profile with  $w_0 = 3.8 \mu\text{m}$  and a Gaussian longitudinal envelope with pulse duration of  $45 \text{ fs}$ . The normalized vector potential  $a_0 = 4.5$ .

*Density matching condition for LWFA.* To better understand the density matching condition for the generation of large charge, energetic and collimated electron beam, we studied the gas density influences on the small focal spot laser wakefield acceleration, as shown in Figs. 4. The drive laser pulse with power  $\sim 30 \text{ TW}$  could not self-focusing in nitrogen gas with density  $4 \times 10^{17} \text{cm}^{-3}$  (corresponding to fully ionized plasma density  $5.6 \times 10^{18} \text{cm}^{-3}$  and  $P_c = 52 \text{ TW}$ ), and its intensity decreases to  $a_0 \sim 1.25$  [Fig. 4(e)] which is lower than the ionization injection threshold of the  $6^{\text{th}}$  electron of nitrogen atom ( $a_0 \sim 1.7$ )[43]. However, due to the initial laser  $a_0 \sim 4.5$  is much higher than that of the  $7^{\text{th}}$  electron of nitrogen atom ( $a_0 \sim 1.9$ ), electrons would experience ionization injection [Fig. 4(a)] in the process

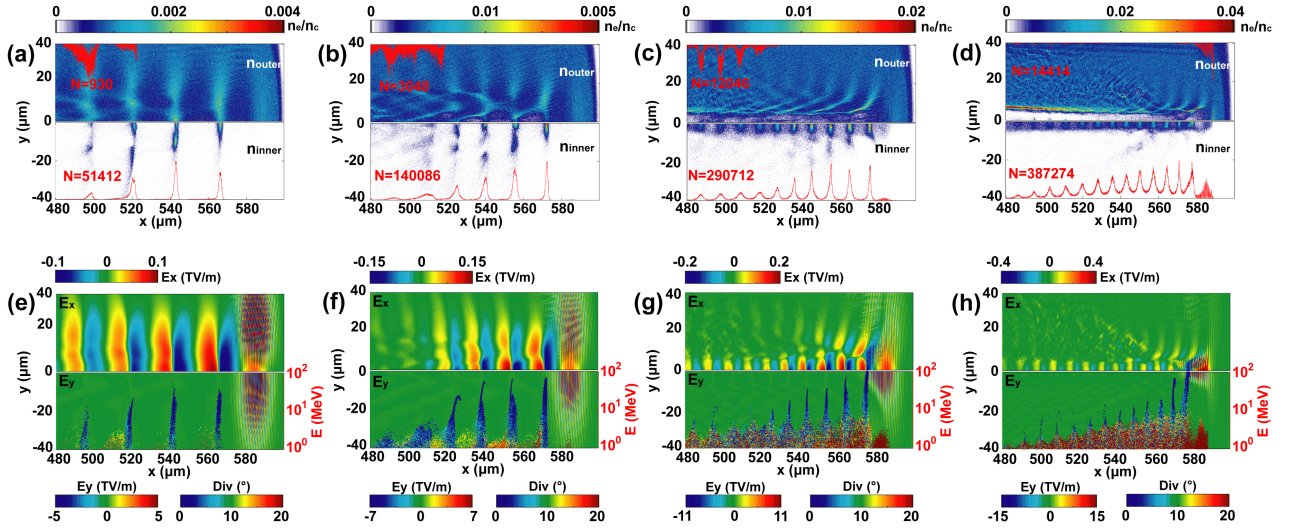


FIG. 4. Small focal spot laser wakefield acceleration in pure nitrogen gas with different densities. (a-d) Plasma electron density distributions, where the upper/down represents the outer/inner shell electrons of nitrogen atom respectively, the red line (peak normalized) is electron number longitudinal distribution for  $E_k \geq 1$  MeV and the number is the corresponding total micro particles. (e-h) Electric-field distributions, where the upper/down represents the  $E_x/E_y$  respectively, the scattering micro represent electron phase-space ( $x - E_k$ ) distribution and the color represents electron divergence angle. (a, e) correspond to nitrogen gas density  $4 \times 10^{17} \text{ cm}^{-3}$ ; (b, f)  $6 \times 10^{17} \text{ cm}^{-3}$ ; (c, g)  $1 \times 10^{18} \text{ cm}^{-3}$ ; (d, h)  $2.2 \times 10^{18} \text{ cm}^{-3}$ .

of laser defocusing until  $a_0$  less than the threshold of the 6<sup>th</sup> electron, then electrons stop injecting as shown in Fig. 4(e). Significantly, many inner shell electrons are ionized and injected into successive multiple bubbles. When the gas density is increased to  $6 \times 10^{17} \text{ cm}^{-3}$ , the corresponding  $P_c \approx 35$  TW is still higher than the power of drive laser, the laser pulse can not self-focusing but with slower defocus speed and keep  $a_0 \sim 1.7$  at the same distance [Fig. 4(f)], which results in more inner shell electrons ionization injection into bubbles [Fig. 4(b)]. If the gas densities continuously increase to  $1 \times 10^{18} \text{ cm}^{-3}$  and  $2.2 \times 10^{18} \text{ cm}^{-3}$  corresponding to  $P_c \geq 21$  TW and 10 TW respectively, small focal spot laser would match to the plasma bubble during the self-focusing process, resulting in the laser intensity easily maintained above the threshold of the 7<sup>th</sup> electron [Figs. 4(g, h)], and more inner shell electrons are injected into over ten bubbles to form high charge beam [Figs. 4(c, d)]. Although the higher density plasma is beneficial to increase the beam charge to a certain extent [Figs. 4(c, d)], the energy gain is lower due to that both the dephasing length  $L_d \propto n_e^{-3/2}$  and the laser pump depletion length  $L_p \propto n_e^{-1}$  are shorter[40] in that cases [Figs. 4(g, h)]. That means we need to keep balance between electron charge and energy. In a word, with a suitable plasma density, the matched small focal spot laser pulse can maintain high intensity above the 7<sup>th</sup> ionization threshold of nitrogen atom, and result in more inner shell electrons ionization inject into plasma wakefields.

In LWFA, the first wakefield or bubble in matched case, is usually more concerned due to the process of

electron injection is more likely to occur inside[47, 48]. However, the number of electrons that can be loaded into a 3D nonlinear bubble is limited by the beam loading effect. According to M. Tzoufras's theory[44], when the drive laser with a matched profile  $k_p R \simeq 2\sqrt{a_0}$ , the maximum charge of loaded electrons  $\frac{Q_s}{1nC} \simeq 0.047 \sqrt{\frac{10^{16} \text{ cm}^{-3}}{n_e}} (2\sqrt{a_0})^4 \frac{m_e c \omega_{pe}}{e E_s}$ . According to the above conditions  $a_0 \sim 4.5$ ,  $n_e \sim 3.68 \times 10^{19} \text{ cm}^{-3}$ , and the acceleration field after reduction due to the beam loading effect  $E_s \sim 0.1$  TV/m [Fig. 4(h)], the bubble can sustain the charge  $Q_s$  could be  $\sim 1.8$  nC. However, in our case of small focal spot LWFA with high laser intensity, laser pulse can excite more wakefields and keep intensity exceeding the ionization threshold of nitrogen inner shell electrons. These electrons can be continuously ionized and injected into over ten bubbles [Fig. 4(g)], which results in the beam charge much higher than the limit of beam loading effect of a single bubble.

*Multiple ionization injections and electron beam evolutions.* To deeply understand the process of multiple ionization injection, the injection condition for the small focal spot LWFA in the nitrogen gas are presented [Figs. 5(a-c)]. Although the laser pulse would evolve due to the effect of self-focusing and etching in plasma, the plasma wake evolution is insignificant during propagating tens of microns. Thus, the electrostatic potential  $\Psi$  of plasma wake can be used to qualitatively discuss the ionization injection conditions[43]. Actually, electrons born at the peak of the wake potential ( $E_z = 0$ ) will experience the largest  $|\Delta\Psi_{max}|$ , if  $\Delta\Psi_{max} < -1$  then electrons will

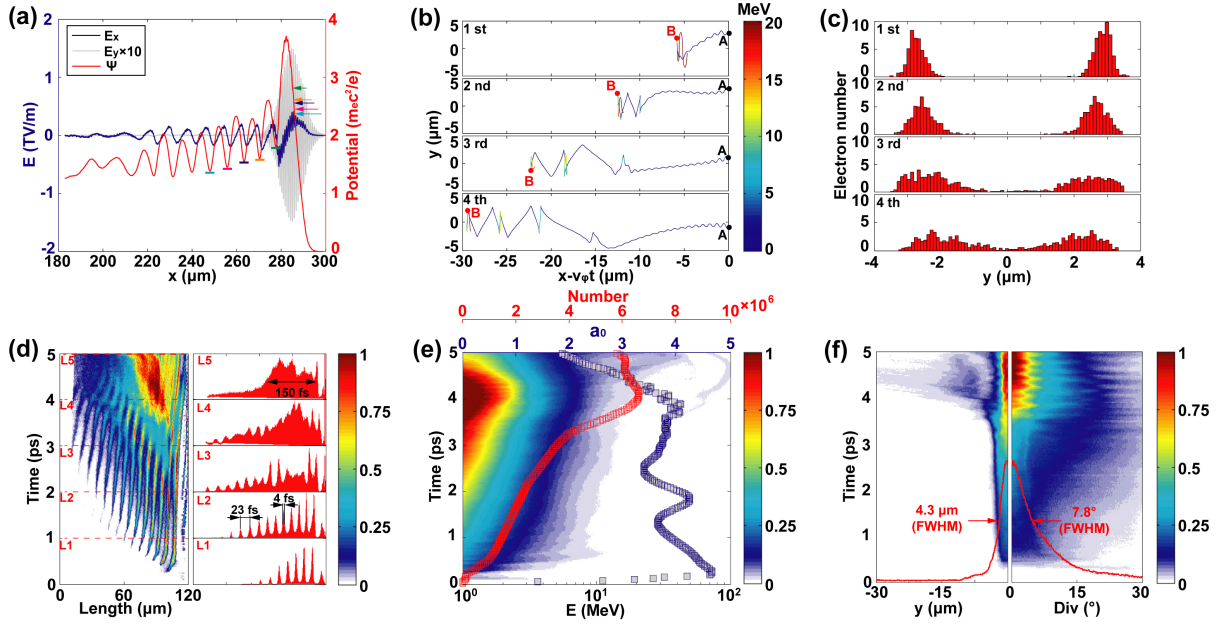


FIG. 5. Analysis of multiple ionization injections and electron beam evolutions. (a) The axial electric-fields ( $E_x$  blue line,  $E_y$  gray line) of laser pulse at the moment of 1 ps and the corresponding electrostatic potential (red line) of  $E_x$ . (b) Four tracked electrons trajectories in the reference frame of drive laser pulse correspond to the 1<sup>st</sup>, 2<sup>nd</sup>, 3<sup>rd</sup> and 4<sup>th</sup> bubble respectively, in which the points A, B represent the position of ionization and injection respectively. (c) The transversal distribution of initial ionization position of electrons selected from 1<sup>st</sup>, 2<sup>nd</sup>, 3<sup>rd</sup> and 4<sup>th</sup> bubble respectively. (d) The evolution of electron beam longitudinal distribution. The right five figures correspond to the moments of 1, 2, 3, 4, 5 ps respectively. (e) The evolution of electrons energy distribution. The blue and red squares represent to the evolution of laser  $a_0$  and total electron micro-particle number ( $E_k \geq 1$  MeV) respectively. (f) The evolutions of transversal distribution and divergence angle of electron beam, in which the two red lines demonstrate the distributions of outgoing electron beam.

be ionized earlier in the wake and can be trapped[42]. The maximum wake potential can be approximated as  $\Psi_{max} \approx \frac{(k_p R)^2}{4} \approx a_0$ , so the higher  $a_0$  is propitious to trap electrons. By contrary, electrons born on pulse rising edge as shown blue arrow in Fig. 5(a), they would not experience a sufficient potential to be trapped in the first bubble. Fortunately, the potential in the subsequent wakefield is lower than the previous one due to the non-linear blowout regime[10, 42], resulting in these electrons could be trapped by the subsequent wakefield. In practice, if the inner shell electrons are ionized transversely far away from the axis of  $y=0$ , they will be longitudinally close to the peak of pulse envelope, and then they would experience sufficient potential to be trapped by the first bubble as shown in “1 st” of Fig. 5(b). However, when the electrons are ionized close to the axis of  $y=0$ , they will be born at the front edge of laser pulse. These electrons would be trapped by more backward wakefields, for example, as shown in “3 rd”, “4 th” of Fig. 5(b). Figure 5(c) demonstrates more intuitively that inner shell electrons ionized transversely close to the  $y=0$  axis are injected into more backward bubbles.

To systematically introduce the characteristics of electron beam, the beam length evolution in plasma channel is presented in Fig. 5(d). At the beginning of LWFA

process, the electron beam longitudinal distribution has many modulation peaks with interval  $\sim 23$  fs and duration  $\sim 4$  fs. As electrons continuously inject into plasma bubbles, these electron bunches begin to combine after  $\sim 3$  ps, then the outgoing electron beam has a duration of  $\sim 150$  fs (in FWHM). Hence the estimated beam peak current is  $\sim 100$  kA, according to the beam average charge of  $\sim 15$  nC in our experiment. Because the limit of dephasing length  $L_d \approx \frac{2\omega_p^2 R}{3\omega_0^2} \approx 120 \mu\text{m}$ , the electron maximum energy gain[40]  $\Delta E \approx \frac{2}{3} m_e c^2 (\frac{\omega_0^2}{\omega_p^2})^2 a_0 \approx 100$  MeV as shown in Fig. 4(h). Because beam loading effect reduces the acceleration electric-field, the energies of most electrons are located in the range of MeV to 30 MeV as shown in Fig. 5(e), which agree well with the experiment results. Due to the existence of self-generated confinement electromagnetic fields in the plasma bubbles[48, 49], the electron beam has small source size (4.3  $\mu\text{m}$ ) and divergence angle (7.8°) as shown in Fig. 5(f).

This kind of tens MeV, large charge, collimated, short duration electron beam has great potential for driving an ultra-high flux photofission neutron source, an ultra-brightness gamma ray radiation source, or exciting and accumulating large amounts of isomers within ultra-short duration and tiny spatial size.

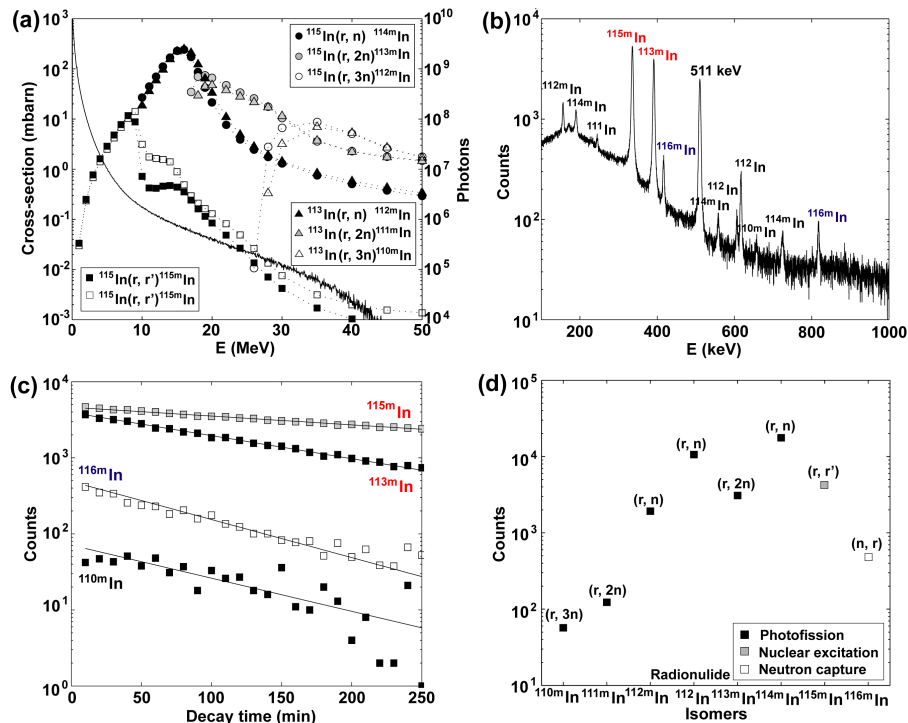


FIG. 6. Results of isomers excitation. (a) The bremsstrahlung spectrum from W converter simulated by Geant4 code (solid line), and the cross-sections of photonuclear reactions from TENDL data library[69]. (b) A typical decay spectrum of In target measured by high pure germanium detector for 250 mins. (c) The experimental decay time spectrums. (d) The single shot yields of isomers and radionuclides produced by different nuclear reactions.

## V. ISOMER EXCITATION RESULTS

Nuclear isomers have a broad range of potential applications[50]. For example, new energy-storage materials[51–54], medical isotopes[55–57], nuclear clocks[58, 59], or nuclear gamma-ray lasers[60, 61]. Especially for nuclear  $\gamma$ -ray lasers whose lifetimes of excited states are needed as short as nanosecond or even shorter[61, 62], due to the relatively large emission linewidth of Doppler broadening, it is a big challenge for traditional accelerators or reactors to pump nuclei to these excited states efficiently[63, 64]. For example, considering a conventional commercial electron accelerator ( $E = 5$  MeV,  $I = 2$  mA, 500 Hz and duration of  $15 \mu\text{s}$ ) shooting on the same converter and target, the peak efficiency of  $(\gamma, \gamma')$  reaction can be estimated to be  $\sim 2 \times 10^7$  p/s. Even, for a traditional high energy electron accelerator (e.g., BEPC-II in China), the estimated peak efficiency could be  $\sim 10^{10}$  p/s for photonuclear reaction  $(\gamma, n)$ . In contrast, the electron beam from LWFA has ultra-high peak current (hundred kA), it has great potential to improve the excitation efficiency of nuclear isomers.

For production of nuclear isomers via photonuclear reactions driven by electron bremsstrahlung radiation, it is efficient for bremsstrahlung photon energy between 5

MeV and 30 MeV, e.g.,  $\gamma$ -ray with energy  $5 \sim 10$  MeV is propitious to drive photonuclear reaction  $(\gamma, \gamma')$  and excite nuclei[65],  $10 \sim 30$  MeV  $\gamma$ -rays are ideal to stimulate giant dipole resonance for photofission reactions  $(\gamma, xn)$  and producing fast neutrons[66] or nuclear isomers[64]. However, for photon energy beyond 30 MeV, the reaction is not effective anymore, as well as the bremsstrahlung photon yield[67].

To experimentally realize efficient photonuclear reactions in In target, a 1 mm thickness W was set close to the nozzle serving as a converter for high brightness  $\gamma$ -ray radiation, and the radiation spectrum [Fig. 6(a)] was simulated by utilizing the above experimental electron beam parameters, the total photon number could be up to  $1 \times 10^{11}$  for  $E_p > 1$  MeV. According to the cross-sections of photonuclear reactions of In, the reactions of  $^* \text{In}(\gamma, \gamma') ^* m \text{In}$ ,  $^* \text{In}(\gamma, n) ^* m \text{In}$ ,  $^* \text{In}(\gamma, 2n) ^* m \text{In}$  and  $^* \text{In}(\gamma, 3n) ^* m \text{In}$  can take place. In this experiment, we utilized electron beam with 0.025 Hz repetition rate to bombard the W+In target for isomer production. After one hour shooting, we took In target out of vacuum chamber, and measured its decay radiation. The decay radiation spectrum is shown in Fig. 6(b), and the different peaks from isomers or radionuclides are marked according to specialized radiation energy referring from NNDC database[68]. Four isomers decay time spectrums

with several hours half-life are shown in Fig. 6(c), and their fitting half-lives agree quite well with the data of NNDC database.

The yield of  $^{115m}\text{In}$  from  $^{115}\text{In}(\gamma, \gamma')^{115m}\text{In}$  is about  $4.16 \times 10^3$  for single shot [Fig. 6(d)]. However, the yield of  $^{114m}\text{In}$  from  $^{115}\text{In}(\gamma, n)^{114m}\text{In}$  could be up to  $1.76 \times 10^4$  due to the higher photofission cross-section. The  $^{113m}\text{In}$  is contributed by  $^{113}\text{In}(\gamma, \gamma')^{113m}\text{In}$  and  $^{115}\text{In}(\gamma, 2n)^{113m}\text{In}$  with the total yield of  $\sim 3.09 \times 10^3$ . The  $^{111m}\text{In}$  excited by  $^{113}\text{In}(\gamma, 2n)^{111m}\text{In}$  has the yield of  $\sim 1.23 \times 10^2$ . Therefore, according to the abundance ratio of  $^{113}\text{In}$  and  $^{115}\text{In}$ , the yield of  $^{113m}\text{In}$  excited from  $^{115}\text{In}(\gamma, 2n)^{113m}\text{In}$  is estimated about  $2.74 \times 10^3$ . In addition, the  $^{116m}\text{In}$  has a yield of  $\sim 4.85 \times 10^2$  from  $^{115}\text{In}(n, \gamma)^{116m}\text{In}$  which is induced by photofission neutrons. Because the gamma ray beam duration is close to the electron beam, the time of  $\gamma$ -ray pass through 3 mm thickness In target is about 10 ps, which can be regarded as the exciting duration time. Therefore, the peak excitation efficiency of isomers from photonuclear reactions are estimated about  $4.16 \times 10^{14}$  p/s ( $\gamma, \gamma'$ ),  $1.76 \times 10^{15}$  p/s ( $\gamma, n$ ) and  $2.74 \times 10^{14}$  p/s ( $\gamma, 2n$ ) respectively. Limited by the vacuum pump efficiency and laser repetition rate in this experiment, the average excitation efficiency of isomer is less than  $5 \times 10^2$  p/s. However, average efficiency  $10^7$  p/s can be realized by utilizing a more powerful pump set and a 100 Hz hundred-TW laser facility which is available right now. This pumping method will also greatly benefit to the production of medical isotopes and nuclear batteries on tabletop.

## VI. CONCLUSION

In summary, we have presented a novel efficient electron injection method in laser plasma wakefield acceleration. The inner shell electrons of nitrogen atom would be continuously ionized injection into multiple bubbles, when the small focal spot intense laser pulse is matched in a suitable higher density nitrogen gas. A hundred kilo-ampere electron beam has been generated with 12.6% energy conversion efficiency from the driving laser. The electron beam has average charge of  $\sim 15$  nC, divergence angle of  $\sim 6^\circ$  and suitable energies for photonuclear reactions. By utilizing this high current electron beam to drive the excitation of nuclear isomers via reactions of ( $\gamma, \gamma'$ ), ( $\gamma, xn$ ), an ultra-high isomer pumping peak efficiency  $\sim 1.76 \times 10^{15}$  p/s has been realized in In target, which is at least five orders of magnitude higher than using traditional electron accelerators. This efficient and easily accessible production method of exciting nuclear isomers during short time could be greatly beneficial for the study of nuclear transition mechanisms and nuclear gamma ray lasers.

## ACKNOWLEDGEMENTS

This work is supported by the Science Challenge Project (TZ2018005), the National Nature Science Foundation of China (11875191, 11805266, 11991073, 11890710, 11721404), the Strategic Priority Research Program of the CAS (XDB1602, XDA01020304), the National Key R&D Program of China (2017YFA0403301).

\* Corresponding author:lmchen@sjtu.edu.cn

† Corresponding author:jzhang1@sjtu.edu.cn

- [1] Tajima T, Dawson JM. Laser Electron Accelerator. Physical review letters 1979, **43**(4): 267-270.
- [2] Geddes CG, Toth CS, Van Tilborg J, Esarey E, Schroeder CB, Bruhwiler D, et al. High-quality electron beams from a laser wakefield accelerator using plasma-channel guiding. Nature 2004, **431**(7008): 538-541.
- [3] Mangles SP, Murphy CD, Najmudin Z, Thomas AG, Collier JL, Dangor AE, et al. Monoenergetic beams of relativistic electrons from intense laser-plasma interactions. Nature 2004, **431**(7008): 535-538.
- [4] Faure J, Glinec Y, Pukhov A, Kiselev S, Gordienko S, Lefebvre E, et al. A laser-plasma accelerator producing monoenergetic electron beams. Nature 2004, **431**(7008): 541-544.
- [5] Leemans WP, Gonsalves AJ, Mao HS, Nakamura K, Benedetti C, Schroeder CB, et al. Multi-GeV electron beams from capillary-discharge-guided subpetawatt laser pulses in the self-trapping regime. Physical review letters 2014, **113**(24): 245002.
- [6] Kneip S, McGuffey C, Martins JL, Martins SF, Bellei C, Chvykov V, et al. Bright spatially coherent synchrotron X-rays from a table-top source. Nature Physics 2010, **6**(12): 980-983.
- [7] Wang W, Feng K, Ke L, Yu C, Xu Y, Qi R, et al. Free-electron lasing at 27 nanometres based on a laser wakefield accelerator. Nature 2021, **595**(7868): 516-520.
- [8] Pomerantz I, McCary E, Meadows AR, Arefiev A, Bernstein AC, Chester C, et al. Ultrashort pulsed neutron source. Physical review letters 2014, **113**(18): 184801.
- [9] Pukhov A, Gordienko S, Kiselev S, Kostyukov I. The bubble regime of laser-plasma acceleration: monoenergetic electrons and the scalability. Plasma Physics and Controlled Fusion 2004, **46**(12B): B179-B186.
- [10] Lu W, Huang C, Zhou M, Mori WB, Katsouleas T. Non-linear theory for relativistic plasma wakefields in the blowout regime. Physical review letters 2006, **96**(16): 165002.
- [11] Maier AR, Delbos NM, Eichner T, Hübner L, Jalas S, Jeppe L, et al. Decoding Sources of Energy Variability in a Laser-Plasma Accelerator. Physical Review X 2020, **10**(3).
- [12] Gonsalves AJ, Nakamura K, Daniels J, Benedetti C, Pieronek C, de Raadt TCH, et al. Petawatt Laser Guiding and Electron Beam Acceleration to 8 GeV in a Laser-Heated Capillary Discharge Waveguide. Physical review letters 2019, **122**(8): 084801.
- [13] Mahieu B, Jourdain N, Ta Phuoc K, Dorchies F, Goddet JP, Lifschitz A, et al. Probing warm dense matter using

- femtosecond X-ray absorption spectroscopy with a laser-produced betatron source. *Nature communications* 2018, **9**(1): 3276.
- [14] Ke LT, Feng K, Wang WT, Qin ZY, Yu CH, Wu Y, et al. Near-GeV Electron Beams at a Few Per-Mille Level from a Laser Wakefield Accelerator via Density-Tailored Plasma. *Physical review letters* 2021, **126**(21): 214801.
- [15] Li YF, Li DZ, Huang K, Tao MZ, Li MH, Zhao JR, et al. Generation of 20 kA electron beam from a laser wakefield accelerator. *Physics of Plasmas* 2017, **24**(2): 023108.
- [16] Yan W, Chen L, Li D, Zhang L, Hafz NA, Dunn J, et al. Concurrence of monoenergetic electron beams and bright X-rays from an evolving laser-plasma bubble. *Proceedings of the National Academy of Sciences of the United States of America* 2014, **111**(16): 5825-5830.
- [17] McGuffey C, Thomas AG, Schumaker W, Matsuoka T, Chvykov V, Dollar FJ, et al. Ionization induced trapping in a laser wakefield accelerator. *Physical review letters* 2010, **104**(2): 025004.
- [18] Couperus JP, Pausch R, Kohler A, Zarini O, Kramer JM, Garten M, et al. Demonstration of a beam loaded nanocoulomb-class laser wakefield accelerator. *Nature communications* 2017, **8**(1): 487.
- [19] Huang K, Li DZ, Yan WC, Li MH, Tao MZ, Chen ZY, et al. Simultaneous generation of quasi-monoenergetic electron and betatron X-rays from nitrogen gas via ionization injection. *Applied Physics Letters* 2014, **105**(20): 204101.
- [20] Mirzaie M, Li S, Zeng M, Hafz NA, Chen M, Li GY, et al. Demonstration of self-truncated ionization injection for GeV electron beams. *Scientific reports* 2015, **5**: 14659.
- [21] Tzoufras M, Lu W, Tsung FS, Huang C, Mori WB, Katsouleas T, et al. Beam loading in the nonlinear regime of plasma-based acceleration. *Physical review letters* 2008, **101**(14): 145002.
- [22] Götzfried J, Döpp A, Gilljohann MF, Foerster FM, Ding H, Schindler S, et al. Physics of High-Charge Electron Beams in Laser-Plasma Wakefields. *Physical Review X* 2020, **10**(4).
- [23] Guillaume E, Döpp A, Thauray C, Lifschitz A, Goddet JP, Tafzi A, et al. Physics of fully-loaded laser-plasma accelerators. *Physical Review Special Topics - Accelerators and Beams* 2015, **18**(6).
- [24] Döpp A, Guillaume E, Thauray C, Lifschitz A, Sylla F, Goddet JP, et al. A bremsstrahlung gamma-ray source based on stable ionization injection of electrons into a laser wakefield accelerator. *Nuclear Instruments and Methods in Physics Research Section A: Accelerators, Spectrometers, Detectors and Associated Equipment* 2016, **830**: 515-519.
- [25] Mirzaie M, Hafz N, Li S, Liu F, He F, Cheng Y, et al. Enhanced electron yield from laser-driven wakefield acceleration in high-Z gas jets. *The Review of scientific instruments* 2015, **86**(10): 103502.
- [26] Mirzaie M, Hafz NAM, Li S, Gao K, Li G, ul-Ain Q, et al. Laser acceleration in argon clusters and gas media. *Plasma Physics and Controlled Fusion* 2016, **58**(3): 034014.
- [27] Modena A, Najmudin Z, Dangor AE, Clayton CE, Marsh KA, Joshi C, et al. Electron acceleration from the breaking of relativistic plasma waves. *Nature* 1995, **377**(6550): 606-608.
- [28] Wagner R, Chen SY, Maksimchuk A, Umstadter D. Electron Acceleration by a Laser Wakefield in a Relativistically Self-Guided Channel. *Physical review letters* 1997, **78**(16): 3125-3128.
- [29] Mangles SPD, Walton BR, Tzoufras M, Najmudin Z, Clarke RJ, Dangor AE, et al. Electron Acceleration in Cavitated Channels Formed by a Petawatt Laser in Low-Density Plasma. *Physical review letters* 2005, **94**(24).
- [30] Albert F, Lemos N, Shaw JL, Pollock BB, Goyon C, Schumaker W, et al. Observation of Betatron X-Ray Radiation in a Self-Modulated Laser Wakefield Accelerator Driven with Picosecond Laser Pulses. *Physical review letters* 2017, **118**(13): 134801.
- [31] Lemos N, Albert F, Shaw JL, Papp D, Polanek R, King P, et al. Bremsstrahlung hard x-ray source driven by an electron beam from a self-modulated laser wakefield accelerator. *Plasma Physics and Controlled Fusion* 2018, **60**(5): 054008.
- [32] Li YF, Feng J, Tan JH, Wang JG, Li DZ, Dong KG, et al. Electron beam and betatron x-ray generation in a hybrid electron accelerator driven by high intensity picosecond laser pulses. *High Energy Density Physics* 2020, **37**: 100859.
- [33] Thévenet M, Leblanc A, Kahaly S, Vincenti H, Vernier A, Quéré F, et al. Vacuum laser acceleration of relativistic electrons using plasma mirror injectors. *Nature Physics* 2015, **12**(4): 355-360.
- [34] Zhou C, Bai Y, Song L, Zeng Y, Xu Y, Zhang D, et al. Direct mapping of attosecond electron dynamics. *Nature Photonics* 2020, **15**(3): 216-221.
- [35] Chopineau L, Leblanc A, Blaclard G, Denoëud A, Thévenet M, Vay JL, et al. Identification of Coupling Mechanisms between Ultraintense Laser Light and Dense Plasmas. *Physical Review X* 2019, **9**(1).
- [36] Ma Y, Zhao J, Li Y, Li D, Chen L, Liu J, et al. Ultrahigh-charge electron beams from laser-irradiated solid surface. *Proceedings of the National Academy of Sciences of the United States of America* 2018, **115**(27): 6980-6985.
- [37] Li S, Shen B, Xu J, Xu T, Yu Y, Li J, et al. Ultrafast multi-MeV gamma-ray beam produced by laser-accelerated electrons. *Physics of Plasmas* 2017, **24**(9): 093104.
- [38] Liu B, Wang HY, Liu J, Fu LB, Xu YJ, Yan XQ, et al. Generating overcritical dense relativistic electron beams via self-matching resonance acceleration. *Physical review letters* 2013, **110**(4): 045002.
- [39] Hussein AE, Arefiev AV, Batson T, Chen H, Craxton RS, Davies AS, et al. Towards the optimisation of direct laser acceleration. *New Journal of Physics* 2021, **23**(2): 023031.
- [40] Lu W, Tzoufras M, Joshi C, Tsung FS, Mori WB, Vieira J, et al. Generating multi-GeV electron bunches using single stage laser wakefield acceleration in a 3D nonlinear regime. *Physical Review Special Topics - Accelerators and Beams* 2007, **10**(6).
- [41] Hosokai T, Kinoshita K, Watanabe T, Yoshii K, Ueda T, Zhidkov A, et al. Generation of relativistic electrons via interaction between ultra-short laser pulses and supersonic gas jet. In: Clayton CE, Muggli P (eds). *Advanced Accelerator Concepts*, vol. 647. Amer Inst Physics: Melville, 2002, pp 628-633.
- [42] Pak A, Marsh KA, Martins SF, Lu W, Mori WB, Joshi C. Injection and trapping of tunnel-ionized electrons into laser-produced wakes. *Physical review letters* 2010, **104**(2): 025003.

- [43] Chen M, Esarey E, Schroeder CB, Geddes CGR, Leemans WP. Theory of ionization-induced trapping in laser-plasma accelerators. *Physics of Plasmas* 2012, **19**(3): 033101.
- [44] Tzoufras M, Lu W, Tsung FS, Huang C, Mori WB, Katsouleas T, et al. Beam loading by electrons in nonlinear plasma wakes. *PHYSICS OF PLASMAS* 2009, **16**(5).
- [45] Giulietti A, Bourgeois N, Ceccotti T, Davoine X, Dobosz S, D'Oliveira P, et al. Intense gamma-ray source in the giant-dipole-resonance range driven by 10-TW laser pulses. *Physical review letters* 2008, **101**(10): 105002.
- [46] Arber TD, Bennett K, Brady CS, Lawrence-Douglas A, Ramsay MG, Sircombe NJ, et al. Contemporary particle-in-cell approach to laser-plasma modelling. *Plasma Physics and Controlled Fusion* 2015, **57**(11): 113001.
- [47] Pukhov A, Meyer-ter-Vehn J. Laser wake field acceleration: the highly non-linear broken-wave regime. *Applied Physics B: Lasers and Optics* 2002, **74**(4-5): 355-361.
- [48] Esarey E, Schroeder CB, Leemans WP. Physics of laser-driven plasma-based electron accelerators. *Reviews of Modern Physics* 2009, **81**(3): 1229-1285.
- [49] Corde S, Ta Phuoc K, Lambert G, Fitour R, Malka V, Rousse A, et al. Femtosecond x rays from laser-plasma accelerators. *Reviews of Modern Physics* 2013, **85**(1): 1-48.
- [50] Arahamian A, Sun Y. Long live isomer research. *Nature Physics* 2005, **1**(2): 81-82.
- [51] Carroll JJ, Burnett J, Drummond T, Lepak J, Propri R, Smith D, et al. Initial Search for Triggered Gamma Emission from  $^{178}\text{Hf}^{m2}$  Using the YSU Miniball Array. *Hyperfine Interactions* 2002, **143**(1-4): 37-54.
- [52] Carroll JJ, Karamian SA, Rivlin LA, Zadernovsky AA. X-Ray-Driven Gamma Emission. *Hyperfine Interactions* 2001, **135**(1-4): 3-50.
- [53] D. Belic, C. Arlandini, J. Besserer, et al. Photoactivation of  $^{180}\text{Ta}^m$  and Its Implications for the Nucleosynthesis of Nature's Rarest Naturally Occurring Isotope. *Physical review letters* 1999, **83**: 5242.
- [54] Wu Y, Keitel CH, Pálffy A.  $\text{Mo}^{93m}$  Isomer Depletion via Beam-Based Nuclear Excitation by Electron Capture. *Physical review letters* 2019, **122**(21).
- [55] Banerjee S, Pillai MRA, Ramamoorthy N. Evolution of  $\text{Tc}^{99m}$  in diagnostic radiopharmaceuticals. *Semin Nucl Med* 2001, **31**(4): 260-277.
- [56] Lee H, Shields AF, Siegel BA, Miller KD, Krop I, Ma CX, et al.  $^{64}\text{Cu}$  Positron Emission Tomography Quantifies Variability of Enhanced Permeability and Retention of Nanoparticles in Relation to Treatment Response in Patients with Metastatic Breast Cancer. *Clinical cancer research : an official journal of the American Association for Cancer Research* 2017, **23**(15): 4190-4202.
- [57] Pan WT, Song T, Lan HY, Ma ZG, Zhang JL, Zhu ZC, et al. Photo-excitation production of medically interesting isomers using intense gamma-ray source. *Applied radiation and isotopes* 2021, **168**: 109534.
- [58] von der Wense L, Seiferle B, Laatiaoui M, Neumayr JB, Maier H-J, Wirth H-F, et al. Direct detection of the  $^{229}\text{Th}$  nuclear clock transition. *Nature* 2016, **533**(7601): 47-51.
- [59] Seiferle B, von der Wense L, Bilous PV, Amersdorffer I, Lemell C, Libisch F, et al. Energy of the  $^{229}\text{Th}$  nuclear clock transition. *Nature* 2019, **573**(7773): 243-246.
- [60] Tkalya EV. Proposal for a Nuclear Gamma-Ray Laser of Optical Range. *Physical review letters* 2011, **106**(16): 162501.
- [61] Rivlin LA, Zadernovsky AA. Nuclear gamma-ray laser: A comparative analysis of various schemes. *Laser Physics* 2010, **20**(5): 971-976.
- [62] Odeurs J, Hoy GR, Rostovtsev Y, Shakhmuratov RN. Towards more relaxed conditions for a gamma-ray laser: Methods to realize induced transparency for nuclear resonant gamma radiation. *Laser & Photonics Reviews* 2010, **4**(1): 1-20.
- [63] Kulko AA, Demekhina NA, Kalpakchieva R, Kolesnikov NN, Lukashik VG, Penionzhkevich YE, et al. Isomeric ratios for  $^{196,198}\text{Tl}$  and  $^{196,198}\text{Au}$  from fusion and transfer in the interaction of  $^6\text{He}$  with  $^{197}\text{Au}$ . *Journal of Physics G: Nuclear and Particle Physics* 2007, **34**(11): 2297-2306.
- [64] Habs D, Köster U. Production of medical radioisotopes with high specific activity in photonuclear reactions with  $\gamma$ -beams of high intensity and large brilliance. *Applied Physics B* 2010, **103**(2): 501-519.
- [65] Carroll JJ, Byrd MJ, Richmond DG, Sinor TW, Taylor KN, Hodge WL, et al. Photoexcitation of nuclear isomers by  $(\gamma, \gamma')$  reactions. *Physical review C, Nuclear physics* 1991, **43**(3): 1238-1247.
- [66] Feng J, Fu C, Li Y, Zhang X, Wang J, Li D, et al. High-efficiency neutron source generation from photonuclear reactions driven by laser plasma accelerator. *High Energy Density Physics* 2020, **36**: 100753.
- [67] Mirani F, Calzolari D, Formenti A, Passoni M. Superintense laser-driven photon activation analysis. *Communications Physics* 2021, **4**(1).
- [68] National Nuclear Data Center. NuDat 3.0. <https://www.nndc.bnl.gov/nudat3/>.
- [69] TENDL-2019 Nuclear data library. Gamma sub-library. [https://tendl.web.psi.ch/tendl\\_2019/gamma.html/gamma.html](https://tendl.web.psi.ch/tendl_2019/gamma.html/gamma.html).